Geophys. J. Int. (2006) **166,** 1363–1367 doi: 10.1111/j.1365-246X.2006.03080.x

Lithospheric thickness beneath the Dabie Shan, central eastern China from *S* receiver functions

F. Sodoudi,[1] X. Yuan,[1] Q. Liu,[2] R. Kind[1,3] and J. Chen[2]

[1] *GeoForschungsZentrum Potsdam, Telegrafenberg,* 14473 *Potsdam, Germany. E-mail: foroug@gfz-potsdam.de*
[2] *Institute of Geology, China Earthquake Administration, Beijing* 100029, *China*
[3] *Freie Universität Berlin, Germany*

Accepted 2006 May 24. Received 2006 May 24; in original form 2006 March 6

SUMMARY

P and *S* receiver functions obtained from a portable array of 34 broad-band stations in east central China provide a detailed image of the crust–mantle and lithosphere–asthenosphere boundaries (LAB) in the Dabie Shan and its adjacent areas. Clear *S*-to-*P* converted waves produced at the LAB show a thin lithosphere beneath the whole study area. Based on our results, the thickest lithosphere of 72 km is observed beneath the southern part of the area within the Yangtze craton, whereas beneath the North-China platform, the lithosphere is only 60 km thick. *S* receiver functions also reveal, in good agreement with *P* receiver functions, a maximum depth of the Moho beneath the Dabie Shan orogen at approximately 40 km. Furthermore, we interpret the structural difference at 32° latitude as the probable location of the mantle suture formed between the Yangtze and the Sino-Korean cratons.

Key words: asthenosphere, crust, lithosphere, mantle, *S* receiver function.

INTRODUCTION

The Qinling-Dabie Shan orogenic belt in central eastern China is exceptional for the widespread occurrence of ultrahigh-pressure (UHP) rocks, which were formed by the Triassic subduction of the northern edge of the Yangtze craton beneath the Sino-Korean craton before or during the collision process and were exhumed to the surface (Fig. 1) (Hacker *et al.* 1995; Grasemann *et al.* 1998). Survival of Archean rocks as well as the presence of diamonds in eastern China are evidence for the nature of a thick cold Archean lithosphere in the Precambrian. However, due to the major thermotectonic change in the lithostratigraphy, which may have started in the early Paleozoic and followed by widespread basin formation throughout the Mesozoic and Cenozoic volcanism, the lithosphere has undergone a process of continued thinning (Menzies & Xu 1998). Detailed knowledge of the lithospheric thickness is an important key to unravel the tectonic history and to understand the tectonic processes. Previous studies were mostly concentrated on crustal structure (Gao *et al.* 1998; Kern *et al.* 1998; Li & Mooney 1998; Wang *et al.* 2000; Schmid *et al.* 2001; Yuan *et al.* 2003; Liu *et al.* 2005) and there are only a few surface wave tomographic studies, which produced useful information on the mantle lid beneath this region (Ekström *et al.* 1997; Huang *et al.* 2003; Priestley *et al.* 2005). Global seismic tomographic inversions indicate that the lithosphere beneath eastern China is significantly thinner than the lithosphere beneath other cratonic blocks; the lithosphere was observed to be thinner than 100 km beneath the Dabie Shan orogen and adjacent regions (Ekström *et al.* 1997; Huang *et al.* 2003; Priestley *et al.* 2005). However, due to low spatial resolution, the tomographic observations could not obtain a detailed image of the lithosphere–asthenosphere boundary (LAB) underneath this area.

A passive seismic array experiment across the Dabie Shan orogenic belt was operated from 2001 April to 2002 March (Liu *et al.* 2005). The temporary network consisting of 34 broad-band seismic stations begins in the south within the Yangzte craton and ends in the north within the Sino-Korean craton (Fig. 1). Technical details are described in Liu *et al.* (2005). *P* receiver function study beneath the Dabie Shan (Liu *et al.* 2005) proposed a complicated pattern for the Moho boundary and suggested several crustal blocks beneath this orogen. In this paper, we apply both the *P* and *S* receiver function methods to the data. Optimal spatial resolution provided by this dense seismic network enables us to estimate the lithospheric structure with higher accuracy and more details than previous attempts. *P* receiver functions resolve the main structure in the crust, whereas *S* receiver functions play a special role in detecting the LAB, which is normally not visible in *P* receiver functions. *S* receiver functions are not influenced by multiples due to the separation of the primary conversions from the multiple phases by the *S* arrival. Thus, the boundaries, which are normally covered by multiples arriving at nearly the same time in the *P* receiver functions, can also be identified in the *S* receiver functions.

THE CRUST–MANTLE BOUNDARY

We calculated *P* and *S* receiver functions for all stations (Fig. 2). We obtained *S* receiver functions using the recently developed technique described, for example, by Kumar *et al.* (2005a,b). A notable

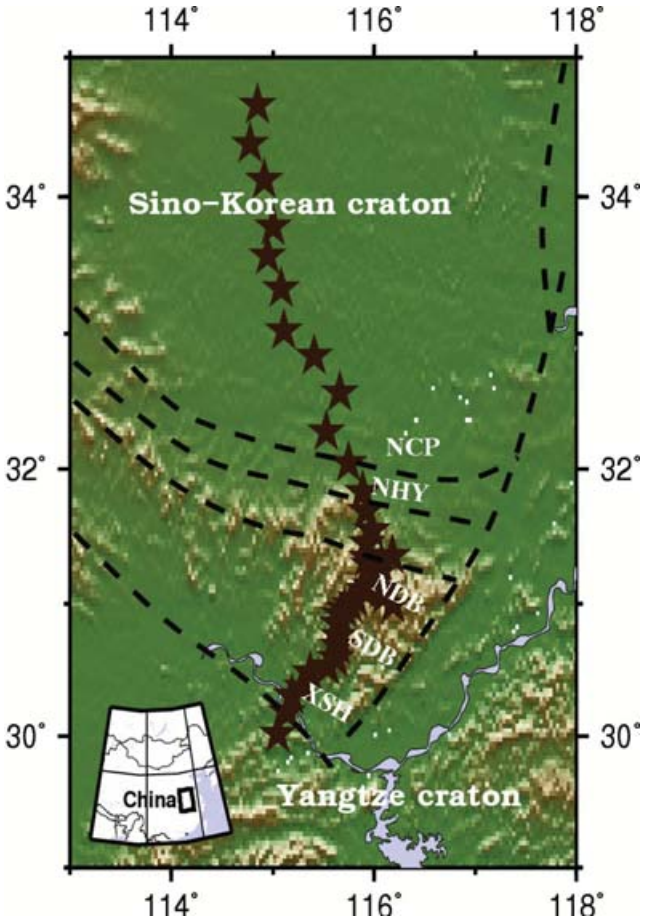

Figure 1. Topographic map of eastern China showing the main crustal blocks across the Dabie Shan orogen and the North-China platform. Main great faults are indicated with dashed lines (Liu *et al.* 2005). Seismic stations are represented by black stars. XSH:Xishui block; SDB:South Dabie Shan; NDB:North Dabie Shan; NHY: North Huaiyang Block and NCP: North-China platform.

difference between the southern and northern parts of the profile can be clearly observed in Fig. 2, both by *P* and *S* receiver functions. Presence of a thick sedimentary layer with a thickness of ∼8 km underneath the North-China platform is an excellent characteristic separating it from the southern part of the area (Fig. 2a). The sediment cannot be well resolved by the *S* receiver functions (Fig. 2b) due to the interference with the Moho at long wavelength. A crustal root beneath the Dabie Shan orogen with a crustal thickness of ∼40 km is clearly resolved by both *P* and *S* receiver functions. The Moho shallows to the south and to the north with a number of offsets, in agreement with reflection and refraction profiles (Wang *et al.* 2000; Yuan *et al.* 2003), recent receiver function study (Liu *et al.* 2005) and Bouguer gravity data (Qiu & Guo 1989; Liou *et al.* 1996). However, *S* receiver functions are not able to resolve the crustal structure beneath the northern part of the area due to their long periods. The Moho multiples are strongly imaged by *P* receiver functions at about 10–15 s arrival time beneath the southern part, whereas in the northern part, complicated upper crustal structure beneath the North-China platform leads to an unclear appearance of Moho multiples (Fig. 2a). A coherent phase with negative amplitude indicating a decreasing velocity with depth (labelled with LAB), can also be observed at about 7–8 s arrival time and may represent *P*-to-*S* converted phases from the LAB (Fig. 2a). The northward continuation of the LAB phase is, however, covered by crustal multiples arriving at the same time.

THE LITHOSPHERE–ASTHENOSPHERE BOUNDARY

To investigate the LAB, we calculated the distribution of the piercing points of *S*-to-*P* conversions at 80 km depth (Fig. 3a). The study region is divided into 19 boxes with respect to the piercing point distribution. The size of each box depends roughly on the number of traces. In the first step, the individual *S* receiver functions are summed in each box. Fig. 3(b) demonstrates the obtained summed traces from the boxes sorted by increasing arrival time of the LAB phase. Two phases are visible in the data. The first phase (in grey) indicates the Moho boundary, while the second stable and coherent phase (in black) is a clear image of the LAB (labelled with LAB). The arrival time of this phase varies between 7 and 9 s. In the second step, we considered a south–north trending profile along the whole area and selected the *S* receiver function stacks, which are located close to this profile, and sorted them by latitude (Fig. 3c). The individual *S* receiver functions along south–north profile are also shown in Fig. 3(d). The Moho and the LAB phases can be well imaged by summed as well as by the individual *S* receiver functions. As Fig. 3(c) shows, notable variations of the LAB phase can be followed along the south–north profile. Beneath the southern part of the profile, it is observed at about 7.5–9 s arrival time (marked with dashed line), whereas beneath the northern part it lies at about 7–7.3 s (marked with dotted line). This difference in the LAB implies that the southern part of the profile located in the Yangtze craton has a thicker lithosphere than does the northern part within the Sino-Korean craton have. The quality of the LAB in Fig. 2(b) is not comparable with the LAB in Fig. 3(c), due to the choice of different low-pass filters (3 and 6 s, respectively).

We convert time to depth using the IASPA91 reference model (Kennett & Engdahl 1991). This procedure may result in a 3.5-km maximum error by the LAB depth estimation, considering a lateral heterogeneity with up to 5 per cent velocity variations in the crust and mantle lithosphere. However, the dominant wave period of the *S* receiver function is larger than 6 s, which corresponds to a wavelength of 25 km. The effect of the 3-D velocity variations on the LAB depth estimates is well beyond the maximum depth resolution power of the *S* receiver functions (∼6 km) and therefore can be neglected. In fact, no large velocity variation in the crust and upper most mantle of the Dabie Shan and adjacent areas was reported before (Huang *et al.* 2003; Wang *et al.* 2000). The LAB depth map (Fig. 4) suggests an important difference in the lithospheric thickness at 32° latitude, which is associated with the northern margin of the Dabie Shan block and beginning of the North-China platform. We interpret this difference in the LAB depth, together with the significant crustal characteristics, as an indication for the presence of various lithospheric blocks, by which the Yangtze lithosphere in the south has a thickness of approximately 70 km, ∼10 km thicker than the Sino-Korean lithosphere in the north.

DISCUSSION AND CONCLUSION

We presented the Moho and LAB obtained from *P* and *S* receiver functions. The maximum thickness of the residual crustal root (only

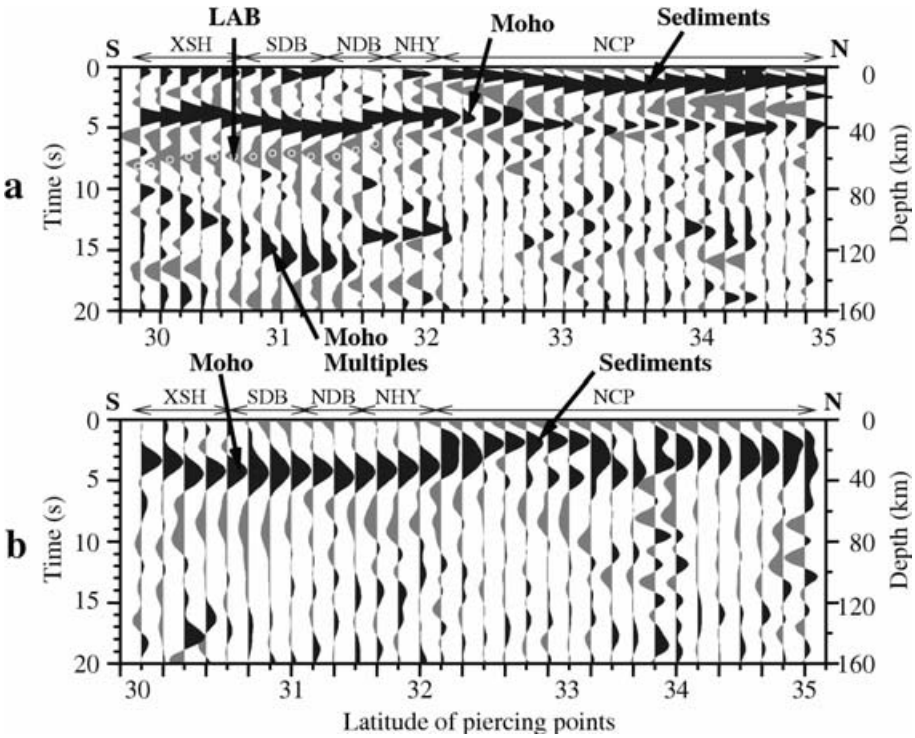

Figure 2. A comparison between crustal structures obtained from *P* (a) and *S* (b) receiver functions. The data were stacked in bins of 0.25° and sorted according to the latitude of their piercing points at 30 km depth. *P* and *S* receiver functions were filtered with bands of 1–20 and 3–20 s, respectively. *S* receiver functions are plotted with reversed polarity in reversed time axis (b) in order to be directly comparable with *P* receiver functions (a). Positive amplitude is plotted in black and negative amplitude is shown in grey. Main crustal blocks along the station profile are also shown at the top (see also Fig. 1). The arrival times of converted waves as well as their corresponding depths (with reference of the IASP91 model) are indicated in the figure. Probable *P*-to-*S* converted phases from the LAB are marked with white circles in (a).

∼6 km) is observed at the southern part of the North Huaiyang Block. This crustal thickening beneath the high elevations of the Dabie Shan orogen (beneath South Dabie Shan, North Dabie Shan in Fig. 2) implies an isostatic balance of the crust, but such a modest crustal root cannot be simply attributed to the significant collisional event occurred in this area. The presence of a thin lithosphere (60–70 km) beneath the main accreted fragments including the Yangtze and the Sino-Korean cratons, as well as the lack of the thick root beneath the Archean crust of the both cratonic blocks suggests that the lithosphere has been thinned and the crust has undergone moderate extension beneath this area. Probable extension, which Dabie Shan has experienced since Mesozoic, together with Cenozoic volcanism occurred in this area (Menzies & Xu 1998) may be responsible for the lithospheric thinning. This interpretation is also supported by high heat flow and extensive seismicity reported presently in this area (Ma *et al.* 1984; Wesnousky *et al.* 1984). Recent global tomographic studies confirmed the lack of the cratonic root and characterized this area with eroded lithosphere and lifted asthenosphere (Ekström *et al.* 1997; Huang *et al.* 2003; Priestley *et al.* 2005). A new *P* receiver function study also reports a similar thinned lithosphere beneath the northern part of the study area (Chen *et al.* 2005). Based on our results, the general pattern of lithospheric variations is quite similar to that of Moho depth variations showing also similar recent tectonic processes which involved the Yangtze craton and the Sino-Korean craton. However, in small scale, distinctive lithospheric characteristics imply the existence of two lithospheric blocks. The resulting LAB depth map shows a good correlation with known geological and tectonic features, separating the Yangtze lithosphere at 32° latitude from the Sino-Korean lithosphere with approximately 60 km thickness in the north. This boundary at 32° latitude may draw the location of the mantle suture between two cratons, which has also been strongly influenced by tectonic processes affecting this area.

ACKNOWLEDGMENTS

The temporary stations were provided by the Institute of Geology, China Earthquake Administration. We would like to thank Dr Ingo Wölbern for data processing, Dr Kurt Wylegalla for field work and Amerika Manzanares for carefully reading the manuscript. We also thank the German Science Foundation (DFG) for supporting this project (grant KI 314/20-1).

REFERENCES

Chen, L., Zheng, T. & Xu, W., 2005. A Thinned Lithospheric Image beneath the Tanlu Fault Zone, Northeastern China: Constructed from Wave Equation Based Receiver Function Migration, AGU Fall Meeting 2005, T41A-1267.

Ekström, G., Tromp, J. & Larson, E.W.F., 1997. Measurements and global models of surface wave propagation, *J. geophys. Res.,* **102**(B4), 8137–8157.

Gao, S., Jin, Z., Jin, S., Kern, H. & Popp, T., 1998. Seismic velocity structure and composition of continental crust in the Dabie- Sulu area, *Contin. Dyn.,* **3,** 108–112.

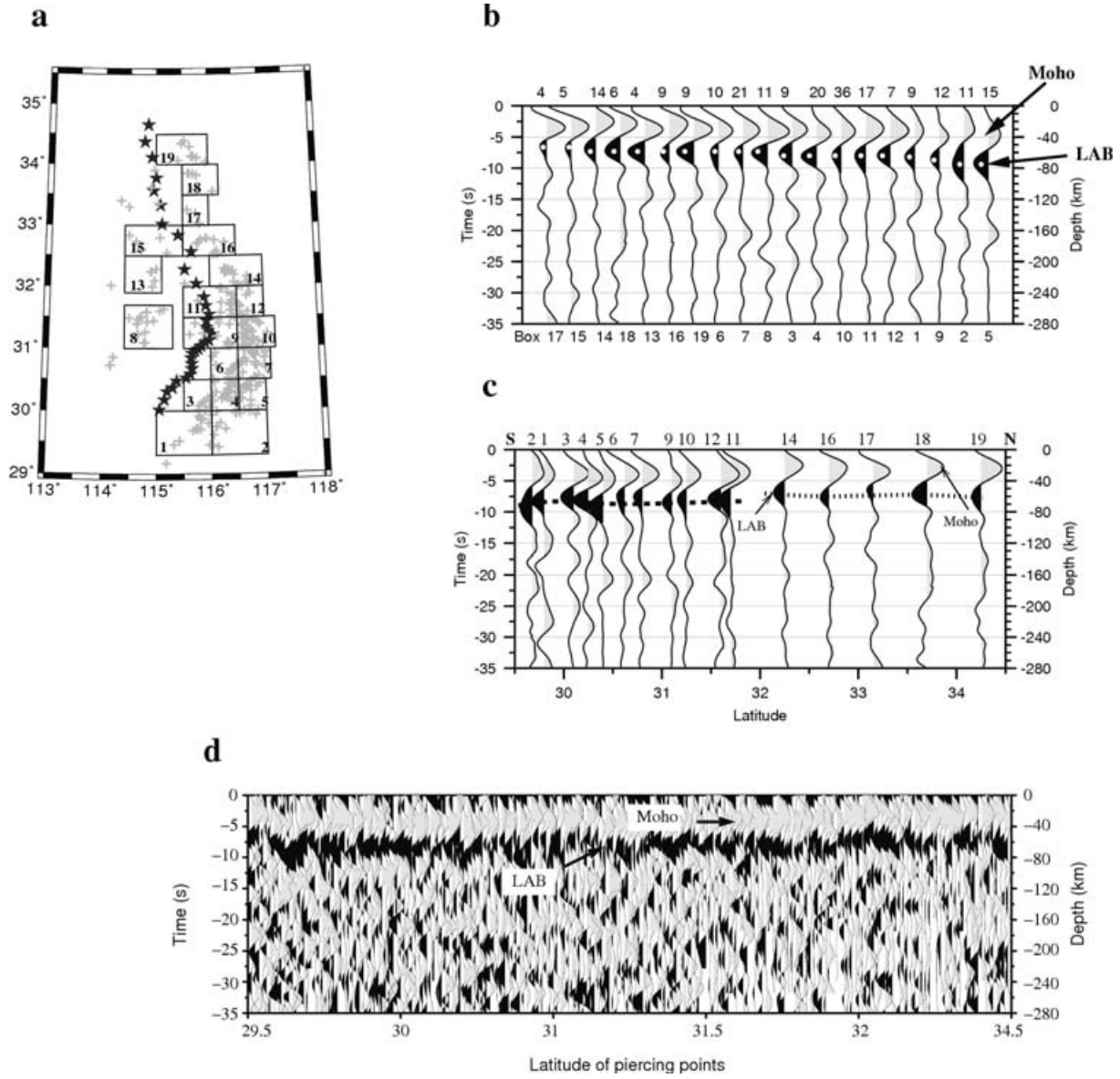

Figure 3. (a) Distribution of the *S*-to-*P* conversions at 80 km depth (approximate depth of the LAB). Location of the seismic stations are shown with black stars. The region has been divided into 19 boxes denoted by numbers. (b) *S* receiver functions were summed in each box. 6-s low-pass filter was used. Depth is converted with reference of the IASP91 model. The box numbers and number of traces in corresponding boxes are shown at the bottom and top panels, respectively. Traces are sorted by the LAB arrival time. Two phases are apparent in the data and are labelled Moho and LAB. (c) *S* receiver function stacks along a south–north profile. Box numbers are indicated at the top of each trace. A structural difference can be observed across 32° latitude. Dashed line beneath the southern part of the profile shows a lithosphere with 70–72 km thickness interpreted as the Yangtze lithosphere, whereas the lithosphere beneath the northern part of the profile (marked with dotted line) is interpreted as the Sino-Korean lithosphere and is slightly thinner. (d) Individual *S* receiver functions sorted by the latitude of their piercing points at 80 km depth along a south–north profile. The conversions from the Moho and the LAB are clearly presented by the data.

Grasemann, B., Ratschbacher, L. & Hacker, B.R., 1998. Exhumation of ultrahigh-pressure rocks: thermal boundary conditions and cooling history, in *When Continents Collide: Geodynamics and Geochemistry of Ultra-high Pressure Rocks,* pp. 117–139, eds Hacker, B.R. & Liou, J.G., Kluwer, Dordrecht.

Hacker, B.R., Ratschbacher, L., Webb, L. & Dong, S., 1995. What brought them up? Exhumation of the Dabie Shan ultrahigh-pressure rocks, *Geology,* **23,** 743–746.

Huang, Z., Su, W., Peng, Y., Zheng, Y. & Li, H., 2003. Rayleigh wave tomography of China and adjacent regions, *J. geophys. Res.,* **108**(B2), doi: 10.1029/2001JB001696.

Kennett, B.L.N. & Engdahl, E.R., 1991. Travel times for global earthquake location and phase identification, *Geophys. J. Int.,* **105,** 429–465.

Kern, H., Gao, S., Jin, Z., Popp, T. & Jin, S., 1998. Petrophysical studies on rocks from the Dabie ultrahigh-pressure (UHP) metamorphic belt, Central China: Implications for the composition and delamination of the lower crust, *Tectonophysics,* **301,** 191–215.

Kumar, P. *et al.*, 2005a. The Lithosphere-Asthenosphere Boundary in the Atlantic Region, *Earth planet. Sci. Lett.,* **236,** 249–257.

Kumar, P., Yuan, X., Kind, R. & Kosarev, G., 2005b. The lithosphere-asthenosphere boundary in the Tien Shan-Karakoram region from *S*

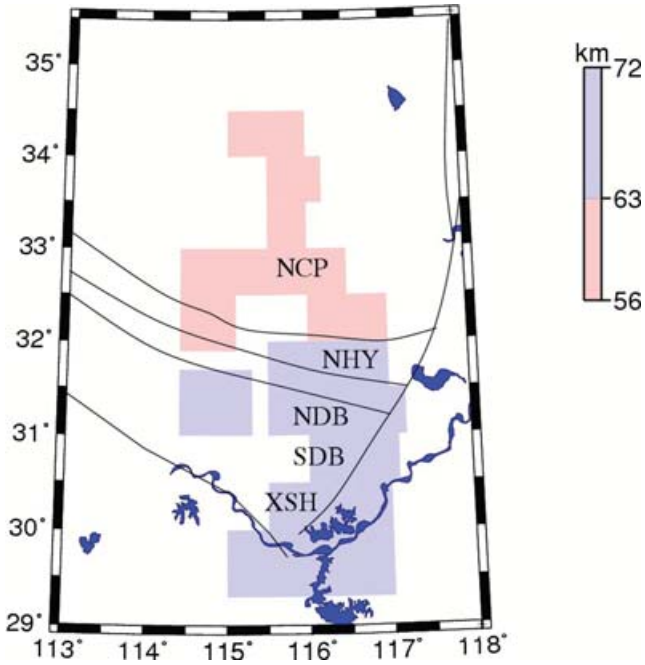

Figure 4. Depths of the LAB for boxes shown in Fig. 3(a). Main crustal blocks are also shown. A boundary at 32° corresponds with the mantle suture, which separates the Yangtze craton lithosphere from the slightly thinner Sino-Korean craton lithosphere.

receiver functions—evidence of continental subduction, *Geophys. Res. Lett.,* **32**(7), 1–4.

Li, S. & Mooney, W.D., 1998. Crustal structure of China from deep seismic sounding profiles, *Tectonophysics,* **288,** 105–113.

Liou, J.G., Zhang, R.Y., Eide, E.A., Maruyama, S., Wang, X. & Ernst W.G., 1996. Metamorphism and tectonics of high-P and ultrahigh-P belts in Dabie-Sulu Regions, eastern China, in *The Tectonic Evolution of Asia,* pp. 300–343, eds Yin, A. & Harrison, T.M., Cambridge University Press, Cambridge.

Liu, Q., Kind, R., Chen, J., Yuan, X., Li, S., Guo, B., Wylegalla, K. & Lai, Y., 2005. Dislocation structure of the crust-mantle boundary and low-velocity body within the crust beneath the Dabie Shan collision orogen, *Science in China,* **48**(7), 875–885.

Ma, X., Liu, G. & Su, J., 1984. The structure and dynamics of the continental lithosphere in north-northeast China, *Annales Geophysicae,* **3,** 620–622.

Menzies, M.A. & Xu, Y., 1998. Geodynamics of the North China Craton, in *Mantle Dynamics and plate Interactions in East Asia, Geodynamics Series,* Vol. 27, pp. 155–165, eds Flower, M.F.J., Chung, S.-L., Lo, C.-H. & Lee, T.-Y., AGU, Washington, DC.

Priestley, K., Debayle, E., McKenzie, D. & Piliduo S., 2005. Upper Mantle Structure of Eastern Asia from Multi-mode Surface Waveform Tomography, *J. geophys. Res.,* submitted.

Qiu, G.H. & Guo, Q.B., 1989. 1:500,000 gravity anomaly mapping of the Dabie Shan area in Hubei, Henan, and Anhui provinces and discussion on the tectonics, *Anhui Geosci. Technol.,* **2,** 53–66.

Schmid, R., Ryberg, T., Ratschbacher, L., Schulze, A., Franz, L., Oberhansli, R. & Dong, S., 2001. Crustal structure of the eastern Dabie Shan interpreted from deep reflection and shallow tomographic data, *Tectonophysics,* **333,** 347–359.

Wang, C.-Y., Zeng, R.S., Mooney, W.D. & Hacker, B.R., 2000. A crustal model of the ultrahigh-pressure Dabie Shan orogenic belt, China, derived from deep seismic refraction profiling, *J. geophys. Res.,* **105**(B5), 10 857–10 869.

Wesnousky, S., Jones, L., Scholz, C. & Adams, D.Q., 1984. Historical seismicity and rates of crustal deformation along the margins of the Orodes block, north China, *B. Seismol. Soc. Am.,* **74,** 1767–1783.

Yuan, X.-C., Klemperer, S.-L., Teng, W.-B., Liu, L.-X. & Chetwin, E., 2003. Crustal structure and exhumation of the Dabie Shan ultrahigh-pressure orogen, eastern China, from seismic reflection profiling, *Geology,* **31**(5), 435–438.